

A Critical Look at the Identifiability of Causal Effects with Deep Latent Variable Models

Severi Rissanen¹ Pekka Marttinen¹

Abstract

Using deep latent variable models in causal inference has attracted considerable interest recently, but an essential open question is their identifiability. While they have yielded promising results and theory exists on the identifiability of some simple model formulations, we also know that causal effects cannot be identified in general with latent variables. We investigate this gap between theory and empirical results with theoretical considerations and extensive experiments under multiple synthetic and real-world data sets, using the causal effect variational autoencoder (CEVAE) as a case study. While CEVAE seems to work reliably under some simple scenarios, it does not identify the correct causal effect with a misspecified latent variable or a complex data distribution, as opposed to the original goals of the model. Our results show that the question of identifiability cannot be disregarded, and we argue that more attention should be paid to it in future work.

1. Introduction

Causal inference, dealing with the questions of when and how we can make causal statements based on observational data, has been a topic of growing interest in the deep learning community recently. On the one hand, causal inference promises to provide traditional machine learning and AI with methods for explainability, domain adaptation, and causal reasoning capabilities in general (Pearl, 2019). On the other hand, many deep learning methods for improving causal inference have been proposed. Some of the models have been designed under the assumption of no unobserved confounding (Shalit et al., 2017; Yoon et al., 2018; Shi et al., 2019), while others utilize latent variables in one way or the other to account for unobserved confounders (Louizos et al., 2017; Rakesh et al., 2018; Wang & Blei, 2019; Pfohl et al., 2019; Madras et al., 2019; Mayer et al., 2020; Chen et al.,

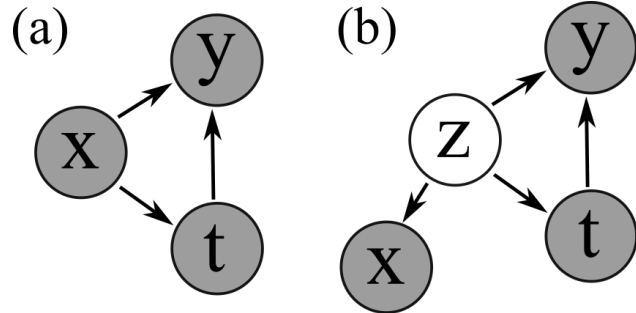


Figure 1. (a) The direct confounding causal graph. (b) The causal graph with an unobserved confounder z , and proxy variables x .

2020; Pawlowski et al., 2020; Jesson et al., 2020; Kim et al., 2020). Although some simple models with unobserved confounders are known to produce correct results (Angrist et al., 1996; Pearl et al., 2016; Miao et al., 2016), the correctness or *identifiability* of causal effects is usually left largely open with deep latent variable models.

In particular, Louizos et al. (2017) proposed the causal effect variational autoencoder (CEVAE) for performing causal inference in the setting where we have an unobserved confounder, of which only noisy proxy variables are available. The causal graph is shown in Fig.1b, which is in contrast to the standard "no unobserved confounding", or direct confounding, graph in Fig.1a. The proxy variable setting has been studied rigorously elsewhere by (Pearl et al., 2016), where the authors provided provably correct methods for a few simple types of data with strong assumptions about the data generating process. They dubbed the process of identifying causal effects in this context as "effect restoration". CEVAE was proposed to relax these assumptions significantly, but the question of identifiability of causal effects was left unanswered.

To provide insight into the identifiability of causal effects with deep latent variable models, we use CEVAE as a case study. CEVAE is a natural choice because it is based on the well-established standard variational autoencoder (Kingma & Welling, 2013; Rezende et al., 2014), and it allows comparison with analytical, provably identifiable methods. We conduct rigorous experiments with the model using various

¹Department of Computer Science, Aalto University, Finland. Correspondence to: Severi Rissanen <severi.rissanen@aalto.fi>.

synthetic and semi-synthetic data sets and also provide theoretical statements in some special cases, offering intuition to the question of identifiability. Even though generic theoretical results are difficult to get for variational autoencoders, we provide conclusions on the assumptions under which the model works or does not work.

2. Preliminaries

2.1. Model description

The objective in the scenario in Fig.1b is to get the causal effect between the variables t and y . t is a variable where we can perform an intervention, e.g., a treatment on a disease. x is the possibly multidimensional proxy and z is the unobserved confounder. The correct interventional distribution $p(y|do(t))$ is defined with the formula

$$p(y|do(t)) = \int p(y|z, t)p(z)dz \quad (1)$$

where the integral is replaced with a sum for a discrete confounder. Note that we denote the latent variable of a VAE with z as well, even though they are conceptually separate and might not be distributed in the same way. The distinction should be clear from the context.

At its core, the causal effect variational autoencoder is simply a regular variational autoencoder with two additional assumptions. First, we assume that the latent variable z corresponds to the unobserved confounder in some way so that after training, we can get the causal effect $p(y|do(t))$ by estimating with the adjustment formula:

$$p(y|do(t)) \approx p_\theta(y|do(t)) = \int p_\theta(y|z, t)p(z)dz \quad (2)$$

where θ are learned decoder parameters and $p(z)$ is the VAE prior. Second, we assert some additional restrictions on the structure of the decoder. The idea is that the quantities reconstructed during training should follow the conditional independencies specified by the causal graph in Fig.1b so that the conditional probability of observed variables given the latent variable factorizes as

$$p_\theta(x^i, t^i, y^i|z) = p_\theta(x^i|z)p_\theta(t^i|z)p_\theta(y^i|z, t^i) \quad (3)$$

where superscript i refers to the i :th observation. Thus, we can write the ELBO for the model as

$$\mathcal{L}(\theta, \phi) = \sum_i [\mathbb{E}_{q_\phi(z|x^i, t^i, y^i)} [\log p_\theta(x^i|z) + \log p_\theta(t^i|z) + \log p_\theta(y^i|z, t^i)] - KL[q_\phi(z|x^i, t^i, y^i)||p(z)]] \quad (4)$$

where x^i, t^i and y^i are observed quantities. This means that we have to define at least four neural networks: The three decoder networks and the encoder network. The original

paper also suggested composing the encoder of multiple networks chosen based on the value of the treatment, but that is not strictly necessary and was not motivated by the causal graph. Note that the decoder differs from usual VAE decoders in that the observed treatment value t^i has to be given as input to the network corresponding to $p_\theta(y|z, t)$. The original paper seemed to suggest that the input should be sampled from the $p_\theta(t|z)$ distribution during training (Fig.2b in (Louizos et al., 2017)), but the factorization in Eq.3 suggests that the observed t should be used instead.

2.2. CEVAE from the point of view of previous work

In terms of the problem statement, CEVAE is perhaps most closely connected to the methods of effect restoration first proposed by Kuroki & Pearl (2014). They offered a provably correct, analytical solution to the proxy variable problem in Fig.1b under some limited circumstances. In particular, they required that x consists of two variables conditionally independent of each other given z . The model variables were also required to be either jointly normally distributed or categorically distributed with an equal number of categories. The setting was further studied in (Miao et al., 2016), where the authors gave conditions on identifiability in a more generic setting, but they did not propose a method to estimate the causal effect.

The fact that CEVAE assumes an entirely different causal graph from the direct confounding graph in Fig.1a has profound implications on the use cases of the model. As shown, e.g., in (Kuroki & Pearl, 2014), the same observed probability distribution $p(x, t, y)$ can map to two completely different causal effects by assuming either the direct confounding or unobserved confounding graphs. Thus, even if the model works perfectly, we can get the wrong result if the actual data generating graph does not conform to the graph in Fig.1b. Likewise, machine learning models that adjust directly to the covariates will fail if the actual data has the unobserved confounder. As even the original paper used data that corresponded to the assumption of no unobserved confounding as their benchmarks, we suspect that this may have been a point of confusion for some.

2.3. Identifiability

In the context of causal inference, we are ultimately interested in the identifiability of causal effects as opposed to the identifiability of the neural networks representing conditional distributions or the identifiability of the latent representation. In particular, identifiability here means that with infinite data, our estimate of $p(y|do(t))$ with Eq.2 should be exact. We focus on whether the model identifies $p(y|do(t))$ instead of individual-level causal effects $p(y|do(t), x)$, because it makes the study of identifiability more straightforward since individual-level esti-

mation is computationally more complicated for CEVAE. Additionally, identifying $p(y|do(t), x)$ implies population level identification as well since we can estimate it using $p(y|do(t)) = \int p(y|do(t), x)p(x)dx$. Note that while the average treatment effect (ATE), defined as $\mathbb{E}[y|do(t = 1)] - \mathbb{E}[y|do(t = 0)]$, is a common metric in other studies, we focus on $p(y|do(t))$ directly because the estimated ATE can have the correct value even if the estimates of $p(y|do(t = 1))$ and $p(y|do(t = 0))$ are not correct.

Conceptually, we can divide the original goals of CEVAE into three:

1. It tries to relax the assumption that we should know the parametric forms of the $p(x|z)$, $p(t|z)$ and $p(y|z, t)$ distributions in advance.
2. It tries to get away with the assumption that we should know the form of the unobserved confounder.
3. It is supposed to work with an arbitrarily complex distribution of proxies.

For the first goal, the hope is that regardless of the actual forms, the neural networks will estimate them correctly or at least correctly enough to identify the causal effect. For the second goal, the hope is that the VAE can somehow represent the confounder with the standard multivariate Gaussian prior so that the causal effects are correctly estimated, even if the true confounder is not normally distributed. Clearly, the second goal is more ambitious, as it requires that the first goal is achieved as well.

In practice, the identification could be prevented by many factors. For real-world data sets, it is possible that the causal effect is not identifiable at all from the data, even if we know the parametric form of the data generating process. If it is identifiable with the right model, CEVAE might still fail due to inherent nonidentifiability caused by the nonparametric assumptions of the model. Local minima or other issues with optimization could cause further practical problems with the correctness of the results.

3. Results

3.1. Setup with simple synthetic data

To gain some confidence on whether CEVAE identifies causal effects in general, we decided to study the simplest possible cases where we know from theory that it is possible to identify the causal effects. These were the data types shown to be identifiable by the effect restoration methods in (Kuroki & Pearl, 2014). Aside from serving as important basic cases, these data sets are interesting because they are relatively simple to study, we can compare CEVAE results to the analytical methods, and because we can try to extract some qualitative understanding from the results.

Linear-Gaussian data The first data type was the linear-Gaussian, where the true data generating distribution is such that all variables are jointly normally distributed, but respecting the conditional independences of graph 2 in Fig.1b. The proxy variable x also consists of two variables x_1 and x_2 that are both conditionally independent on z :

$$z \sim N(0, 1), x_1|z \sim N(c_1 z, \sigma_{x_1}), x_2|z \sim N(c_2 z, \sigma_{x_2}) \\ t|z \sim N(c_t z, \sigma_t), y|z, t \sim N(c_y z + c_y t, \sigma_y)$$

Here, c_i and σ_i are predefined parameters. To avoid jumping to conclusions based on arbitrary choices of data generating parameters, we sampled them randomly from a distribution that should provide a wide range of different generating processes. We detail the sampling method in the Supplementary Material. Note that it is not strictly necessary to assume any specific location and scale of the z distribution to identify the causal effect since we integrate over z when calculating $p(y|do(t))$. Hence, we used $N(0, 1)$ for simplicity.

Binary data In the other type of data, all variables were binary, and in particular, x consisted of two binary variables x_1 and x_2 that were conditionally independent given z . We sampled the data generating process from a distribution explained in the Supplementary Material. The binary data also tests the ability of CEVAE to perform correctly even if the assumption of a normally distributed unobserved confounder is not valid.

To estimate the correctness of causal effect estimates using neural networks with the linear-Gaussian data, standard metrics such as ATE error do not apply because we do not have a binary treatment variable. Instead, we define the *Average Interventional Distance* (AID):

$$AID = \int p(t) \int |p_\theta(y|do(t)) - p(y|do(t))| dy dt \quad (5)$$

where the integrals can be changed to sums for discrete variables. It is simply the L_1 distance between the interventional distribution learned by the model and the true interventional distribution, averaged over treatments with weights according to the current treatment policy. In addition to being defined for continuous treatments, this metric has the advantage that it will only approach zero if $p_\theta(y|do(t))$ approaches $p(y|do(t))$ for all values of t that we have data from. In contrast, the ATE error can approach zero even if this does not happen. It also follows the intuition that we should be more confident for values of t for which we have lots of data.

Estimation models In the experiments, we trained the full CEVAE model to estimate the causal effects, where we parameterized all conditional distributions with MLPs with three layers of width 30 and used a latent variable dimension of 10. With the linear-Gaussian data, standard deviations were individually estimated for each data point with the

standard assumption of diagonal covariance. For comparison, we also considered simple estimation models that matched the data generating distributions more closely. For the linear-Gaussian data, we defined models with conditional distributions represented by simple linear layers and a single common standard deviation estimated for all conditionals. We trained these simple linear-Gaussian estimation models with a latent dimension of one and two. We provide further details in the Supplementary Material.

3.1.1. RESULTS WITH LINEAR-GAUSSIAN DATA

It is, in fact, possible to show that the one-dimensional linear CEVAE is identifiable in this situation, as encapsulated in the following proposition:

Proposition 1. *A linear CEVAE with a one-dimensional latent space identifies the true causal effect, given that it reaches the global optimum of the ELBO with infinite data.*

The proof, which relies on the earlier result by (Kuroki & Pearl, 2014), is provided in the Supplementary Material. Thus, a well-specified CEVAE model can result in correct identification. The question then remains whether overparameterization by neural networks breaks the identifiability, which is what we set out to investigate in this section.

Figure 2a shows the AID of the different models and the analytical method of (Kuroki & Pearl, 2014) as a function of sample size, for one data generating distribution. Analytical estimates for some of the required parameters for calculating $p(y|do(t))$ were not provided in the original paper, but we derive them in the Supplementary Material. We see that while the analytical method and the linear CEVAE with a 1D latent variable perform better than the full CEVAE, all of them seem to converge towards the correct $p(y|do(t))$ distribution. We show in the Supplementary Material that the result is robust, as the estimates converge to the correct distribution for other data-generating parameters. Thus, the experiment provides us evidence that overparameterizing the conditional distributions with NNs or using a larger than required latent variable dimension doesn't necessarily break the identification of the causal effect.

To highlight that the result is not obvious, we ran additional experiments with a model using linear conditional distributions but with a two-dimensional latent space, i.e., with one redundant dimension. With some initializations, the model ended up in a minimum that resulted in a completely wrong causal effect (c_{yt} was estimated to be -0.26 while the true value was -0.62), but an identical ELBO compared to a model with the correct causal effect. We detail the initialization and plot the ELBO and resulting causal effect estimates in the Supplementary Material. Figure 2b visualizes the minimum with the wrong result. Essentially, the problem is that the model uses one latent dimension to reconstruct

the proxies x while treatment t and outcome y are reconstructed partly with the other dimension as well, in which case the dependence between x and t and y is not properly modeled by the latent variables. However, in practice, with a random initialization, this happens only rarely and not at all with the full CEVAE due to the tendency of posterior collapse in VAEs, causing the shared variation of the variables to be modeled using one dimension only, as shown in Fig.2c. Hence, whereas the posterior collapse is often an unwanted characteristic of VAEs (He et al., 2019; Razavi et al., 2019; Dai et al., 2020), it here seems to save the day, although an unnecessarily high latent dimension could still cause issues in principle. We visualize the posterior collapse phenomenon for the full CEVAE in the Supplementary Material.

Conclusion Overparameterization with neural networks does not necessarily break identification, but a too high-dimensional latent variable could in principle. Posterior collapse usually resolves the problem, however.

3.1.2. RESULTS WITH BINARY DATA

The AIDs of the full CEVAE model and the analytical method by (Miao et al., 2016) are plotted as a function of sample size for one data generating distribution in Fig.2d. CEVAE, which incorrectly assumes a Gaussian latent variable, produces reasonable results but fails to converge to the correct causal effect. In contrast, when using the analytical method by (Miao et al., 2016), the estimate gets better and better as the sample size increases. The different convergence of causal effects is demonstrated in Figs.2e and 2f. We show in the Supplementary Material that similar results are obtained for different data generating distributions. Note that the binary data generating process is possibly the simplest possible process where the actual confounder is not normally distributed and the causal effects are identifiable. We conclude that even though CEVAE may produce decent results for some data sets, it does not, in general, identify the true causal effect when the latent variable is not specified correctly in advance. Thus, in practice, it seems necessary to assume the distribution of the unobserved confounder correctly, and the second goal of CEVAE, mentioned in Sec.2.3, is not met. In the Supplementary Material, we also present results for a version of CEVAE with a binary latent variable and show that it can also produce correct causal estimates. It is prone to get stuck in local minima for some data sets, however.

Conclusion CEVAE does not identify the correct causal if the latent variable is misspecified, in general.

3.2. Illustration of difficulties with complex data

This section describes two additional experiments with synthetic data that illustrate issues that could come up with

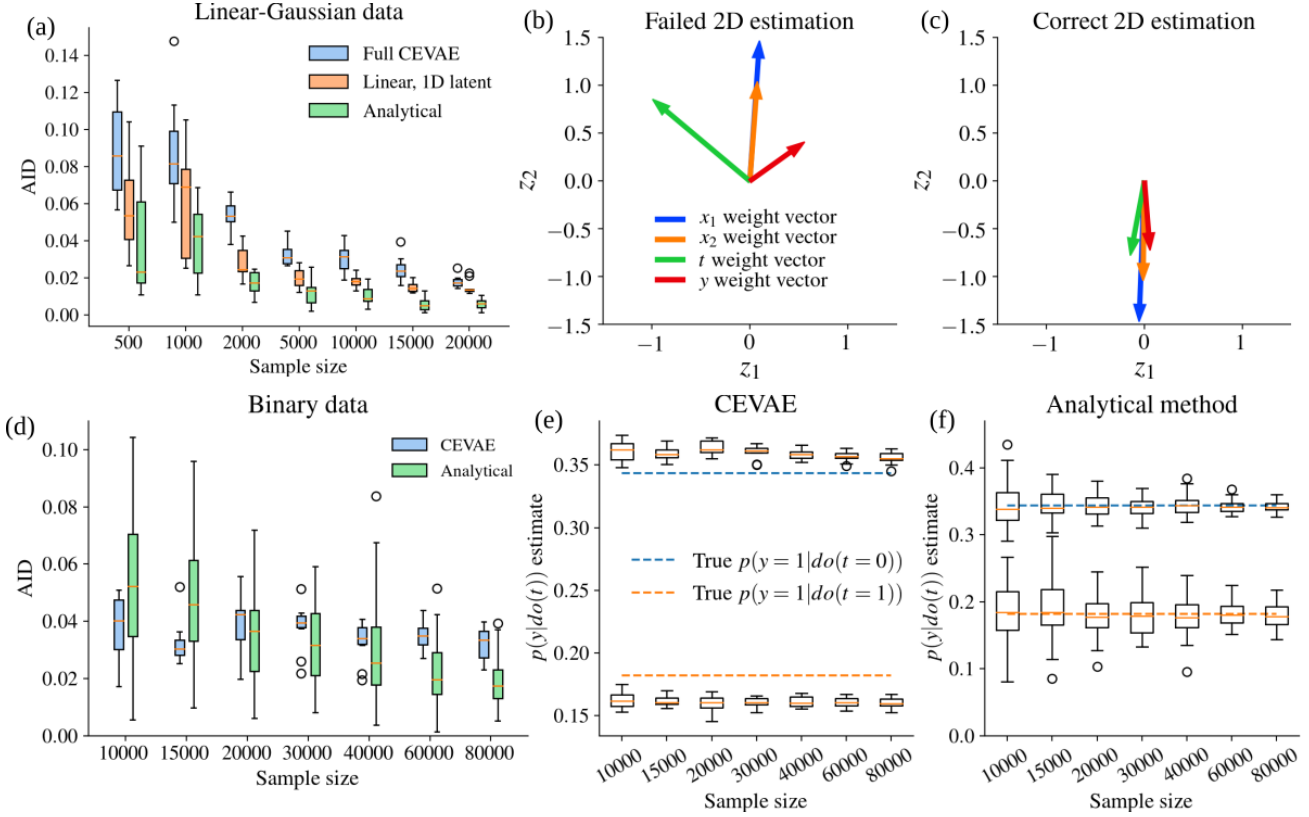


Figure 2. Top row, linear-Gaussian generative model: (a) AID values for the full CEVAE (NN conditionals and 10D latent space), CEVAE with linear conditionals and 1D latent space as well as for the analytical method. (b) Weight vectors of the different conditional distribution mean functions for a linear CEVAE with a two-dimensional latent space. Here parameters were initialized manually, and estimation failed. (c) The same parameter estimates for a model that got the correct causal effect. Bottom row, binary generative model: (d) AID values for the full CEVAE and the analytical method by (Miao et al., 2016), with respect to sample size. (e) Estimates of the $p(y|do(t))$ values for full CEVAE. (f) The same estimates with the analytical method.

real data. The estimation model is the same as the full CEVAE as specified in the previous section unless mentioned otherwise.

3.2.1. DATA WITH IRRELEVANT VARIATION

The former experiments with linear-Gaussian data showed promising results, but it was also clear a multidimensional latent variable was unnecessary for such data. To see how a higher-dimensional latent variable could be necessary with real data, we used the linear-Gaussian data set but added a third proxy variable that contained irrelevant, high-variance noise. We modified the data generating process so that after generating the proxies, an additional rotation was applied to them in the three-dimensional space so that the relevant variation was "hidden" in a specific two-dimensional subspace. The process is illustrated in Fig.3a. Here, with the standard assumption of diagonal covariance in the decoder, we can expect a 1D CEVAE to just model the noise because that dominates the loss. In contrast, a higher-dimensional CEVAE has the option to explain the noise with one and the

signal with another dimension, enabling correct inference.

Figure 3b shows the full CEVAE AID as a function of sample size for one- and two-dimensional latent variables. As expected, the model with a two-dimensional latent variable identifies the true causal effect, while the one-dimensional model does not.

Conclusion A high-dimensional latent variable can be necessary to identify causal effects using very noisy proxies, even if the actual confounder is one-dimensional.

3.2.2. DATA WITH REPEATED PROXIES

The second difficulty in complex data can arise when the proxies contain variation relevant to predicting t and y , but that variation is repeated. As an example, we consider the linear-Gaussian data set, but with a modification that we add two proxies, which are copies of the original two. We also add a small Gaussian noise to the copies to make the situation more realistic. The used estimation model was the full CEVAE, except that we used a linear predictor for the

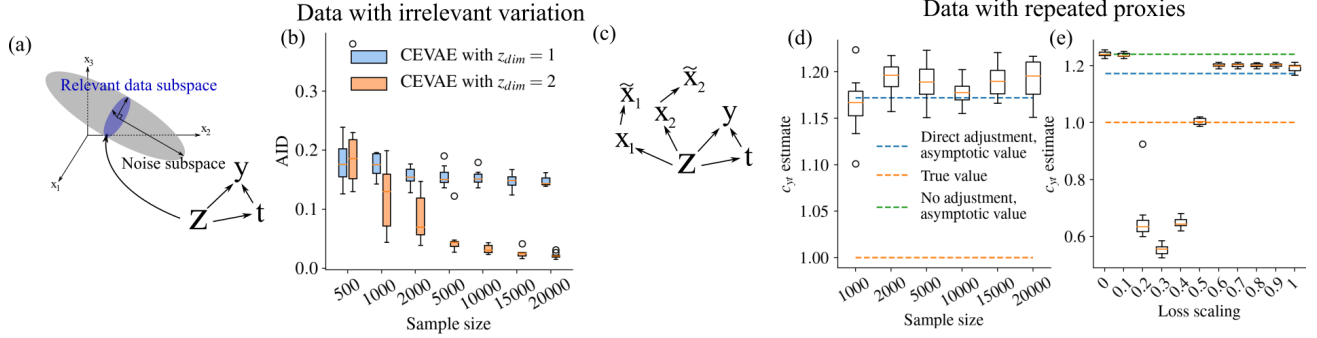


Figure 3. (a) Illustration of the linear-Gaussian data generating process with irrelevant noise and a "hidden" relevant subspace. (b) AID values with respect to sample size for models using one and two-dimensional latent spaces for the data with irrelevant noise. (c) Illustration of the data generating process for linear-Gaussian data with copies \tilde{x}_1 and \tilde{x}_2 . (d) Linear, 1D CEVAE c_{yt} estimate as a function of sample size for the linear-Gaussian data with copies. (e) The c_{yt} estimates as a function of proxy loss scaling for the linear 1D CEVAE.

conditional distribution of y to make the results easier to interpret (the estimated regression coefficient of t should approach the c_{yt} coefficient in the data generating process). Figure 3d shows the c_{yt} estimate as a function of sample size. Instead of approaching the true value, the estimate is closer to the value we would get if we assumed direct confounding by the proxies x instead of the latent z , that is, $p(y|do(t)) = \int p(y|x, t)p(x)dx$ instead of Eq.1, and estimated the value of c_{yt} directly with linear regression.

The reason that CEVAE fails here is that it puts too much weight on the proxies during optimization. In fact, for a data set where we do not add the additional noise to the copies, the following proposition holds:

Proposition 2. *When data are Linear-Gaussian and proxies are copied at least once, the value of the ELBO approaches infinity if we use the latent space to reconstruct the proxies as accurately as possible.*

The proof is included in the Supplementary Material. It is based on the fact that whenever the model reconstructs one of the proxies, it can easily reconstruct the copy as well with the same accuracy. The loss function is then essentially identical to the regular linear-Gaussian data loss function, except that the x reconstruction loss is doubled. When we include the additional noise, the same happens approximately so that the copy can be reconstructed almost as accurately as the original. In both cases, when the latent space is used merely for representing the proxies, the reconstruction loss for y causes the $y|z, t$ predictor to adjust directly for the proxies, albeit in a roundabout way. We hypothesize that this phenomenon will be an issue with a complicated distribution of proxies since, most likely, there will be similar correlations that can cause the model to focus too much on proxy reconstruction.

Given the correspondence of the loss function to the regular linear-Gaussian loss function with proxy reconstruction loss

scaled by a factor of two, the most obvious way to solve the problem seems to be to adjust the reconstruction loss manually by a factor of one-half. In general, we would scale the term $\mathbb{E}_{q_\phi(z|x^i, t^i, y^i)}[\log p_\theta(x^i|z)]$ in Eq.4 by some factor $\lambda < 1$. Intuitively, we would then force the VAE to put less weight on just reconstructing the proxies accurately and take the reconstruction of t and y into account as well. However, in a real-world situation, it is not obvious what this scaling factor should be. To illustrate the effect of the scaling factor on the results, Figure 3e shows the c_{yt} estimate as a function of proxy loss scaling for a sample size of 20000. With scaling factors close to one, the results are close to the direct adjustment results for the reasons explained. When lowering it to one half, the estimate abruptly changes and ends up in the true value, as expected. When lowering it further, however, the results change as well. As the scaling factor approaches zero, CEVAE becomes unable to use the proxy data at all. Here, one global optimum to the ELBO is got by not even trying to adjust to the confounder, as stated in the following proposition:

Proposition 3. *With the proxy reconstruction loss scaled to zero, one global optimum to the ELBO is such that $p_\theta(y|do(t)) = p(y|t)$ for the linear-Gaussian data.*

The proof is in the Supplementary Material. While other global optima exist, it seems that we get the no-adjustment solution in practice due to the tendency of posterior collapse in VAEs, leading the model to choose the solution where the latent space is ignored.

Conclusion CEVAE can overemphasize modeling of the proxies with some data sets, leading it to ignore the unobserved confounder entirely. We may be able to fix this by scaling the reconstruction loss for proxies, but it is not clear how to choose the scaling.

3.3. Semi-synthetic data

Here we describe two experiments based on real-world data sets. Details on the experimental setup and especially the neural network architectures are provided in the Supplementary Material.

3.3.1. PROXY IHDP DATA SET

In this section, we investigate the method's performance on a modified version of the Infant Health and Development Program (IHDP) data set, which was created from a study on the effects of specialist visits and intensive child care on future test scores of premature infants (Hill, 2011). It contains information on 25 covariates, some continuous and some categorical, as well as treatments and generated test scores. The IHDP data is a well-known benchmark for evaluating causal inference with machine learning methods, but as such, it is not suitable for our study for two reasons. First, it is very small with just 747 subjects, which prevents detailed experimentation with NN models. More importantly, the data set is semi-synthetic so that y values are generated directly based on the covariates. As such, the data follows the direct confounding graph instead of the graph assumed by CEVAE. To circumvent the first problem, we trained a variational autoencoder on the covariates to generate more data from a distribution that is similar to the original one and should be realistic enough for our purposes. To solve the second problem, we defined one of the covariates as the hidden confounder, leaving the rest as proxies. We then generated the treatment values by first fitting a feed-forward neural network from the hidden confounder to the treatment values in the original data set and then sampling the treatments based on the probability given by the neural network. The y values were then generated by $y^i = z^i + t^i \cdot \text{ATE} + \epsilon^i$, where ϵ^i is Gaussian noise with a standard deviation of 1 and ATE is the average treatment effect, which was also set to 1. Note that even though the proxies aren't generated from the unobserved confounder, the data set is Markov equivalent to the graph in Fig.1b. The generated data set has the benefit that the distribution of the unobserved confounder and the proxies is not arbitrarily defined but instead follows a real-world distribution that is also relevant for causal inference.

Figure 4a shows the convergence of the causal estimate with respect to sample size. Since the $p(y|do(t))$ estimates get closer to the values we get by adjusting directly for the proxies, it looks like the latent representation is used mainly for proxy reconstruction, and CEVAE is unable to recover the correct causal effect. Is there any hope of recovering the correct causal effect by scaling the proxy reconstruction loss, as suggested by the experiments in Section 3.2.2? This is investigated in Fig.4b, where we plot the causal effect estimates with respect to the scaling factor for one data set

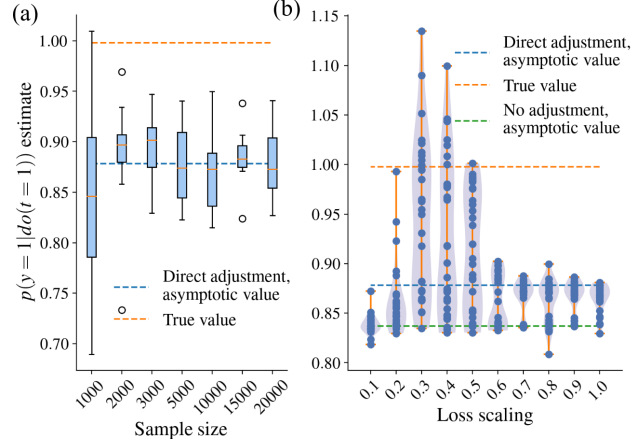


Figure 4. Results for the proxy IHDP data. (a) $p(y = 1|do(t = 1))$ estimates for the IHDP data with respect to sample size. (b) $p(y = 1|do(t = 1))$ estimates for the IHDP data as a function of proxy loss scaling. The figures with $p(y = 1|do(t = 0))$ are included in the Supplementary Material.

of size 20000. The general pattern is that with loss scaling factors close to one, the model essentially adjusts directly for the proxies, and close to zero posterior collapse happens, and y is predicted solely based on t , without confounding. In the middle, some estimates are indeed close to the correct value, but they are not consistently so for any of the scaling factors, in contrast to the repeated linear-Gaussian data.

Conclusion The problem of adjusting directly to the proxies described in Sec.3.2.2 happens with real data.

3.3.2. PROXY MNIST DATA SET

In this section, we experiment with a data set where the proxies are images, which makes sense for CEVAE in the sense that neural networks are a natural choice in this domain. To create data that follows the correct causal graph, we trained a GAN with a three-dimensional latent variable (used as the unobserved confounder) on the MNIST data set, after which we used the GAN to generate a value between zero and one for each pixel given the latent value. We interpreted these as probabilities and sampled each pixel from the corresponding Bernoulli distribution to generate noisy images, which were used as the proxies. Otherwise, we could just as well have adjusted directly for the proxies, and CEVAE would not have been necessary. We then generated t and y values based on the first of the three latent dimensions for each sampled image. The created data set, illustrated in Fig.5a, then followed the correct causal graph with a normally distributed unobserved confounder. Additionally, the other two dimensions of the unobserved confounder contained redundant variation, which CEVAE should be able to take into account with a high-dimensional latent variable. The t and y values were Bernoulli distributed with a probability

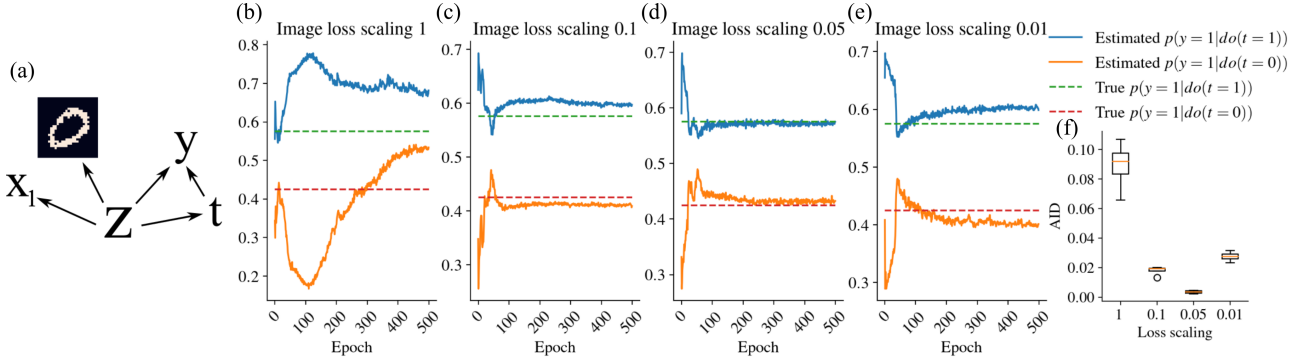


Figure 5. (a) The data generating process for the proxy MNIST data set. (b)-(e): The estimated $p(y|do(t))$ w.r.t. training epoch for different image reconstruction loss scaling values. (f) The AID at epoch 500 for each loss scaling, but run multiple times.

dictated by the value of the unobserved confounder through a logistic link function:

$$\begin{aligned} t|z &\sim \text{Bern}(\sigma(a_t z + b_t)) \\ y|z, t &\sim \text{Bern}(\sigma(a_{y,1}z + b_{y,1})t + \sigma(a_{y,0}z + b_{y,0})(1-t)) \end{aligned}$$

Figure 5b shows the estimated $p(y|do(t))$ values with respect to training epoch for the model. The estimates do not seem to converge to anything even with 500 epochs, indicating that optimization itself can be an issue. An intuitive explanation is that the scale of the image reconstruction loss is much larger than the scale of the other losses, and the model focuses solely on explaining the variation in the images. In light of this and the previous success with scaling proxy losses, we decided to repeat the experiment with the reconstruction loss of the image scaled by different factors. Panels c-e in Fig.5 depict the results. The estimates converge for all scaled image losses but are slightly off for values 0.1 and 0.01. For image loss scaling 0.05, however, we recover almost exactly the correct result. Panel f confirms the result with AID values from multiple runs. Thus, it seems that scaling the loss function appropriately can result in the correct causal effect even with data as complex as images, if we know the correct scaling.

Conclusion With very complex proxy data, getting an estimate for the causal effect can be difficult. In some cases, scaling the loss function by an appropriate factor can result in correct identification even with real data.

4. Discussion

One of the original three goals of the causal effect variational autoencoder, listed in Sec.2.3, was that it should recover the causal effects even if we do not know anything about the confounder's distribution. It was also targeted at the surrogate-rich setting, where we have lots of proxies with a potentially complicated distribution. It appears that CEVAE does not work correctly in either case. Although there is an

absence of theory supporting identification in general, these results were non-obvious to us, and given the large amount of research put into causal inference with similar models, we believe that they are useful for many others. Additionally, in some cases, the model performed even surprisingly well. In particular, in the case of linear-Gaussian data, it does seem to identify the correct causal effects reliably even though the conditional distributions are overparameterized by neural networks and the latent variable dimension is unnecessarily large.

Thus, while using a deep latent variable model in this context shows some promise, new solutions have to be invented to overcome the issues that come up with real data. In particular, scaling the loss function appropriately or some similar trick may result in correct identification, but the challenge is that in contrast to machine learning in general, the true causal effect is not available in the training data. This means that methods like cross-validation can not be used. While the model does not identify the correct causal effect under a misspecified latent variable, it is nevertheless possible that it produces better estimates than a direct adjustment to the proxies, and this could be researched further in the future.

Finally, our aim is not to discourage research with CEVAE or deep latent variable models for causal inference in general, but instead, we hope that our results will accelerate progress in the field. Although we conducted our experiments on CEVAE, we believe that some of the qualitative results and recognized problems will be useful in research on other, similar models. The hope is that our results are a starting point for thinking about identifiability and advancing guarantees for it. In any case, our experiments showed that we should not brush off the question of identifiability entirely since the alternative is that the model can produce incorrect results even with some rudimentary data sets.

References

Angrist, J. D., Imbens, G. W., and Rubin, D. B. Identification of causal effects using instrumental variables. *Journal of the American statistical Association*, 91(434): 444–455, 1996.

Chen, Z., Edwards, A., Hicks, C., and Zhang, K. Inferring personalized and race-specific causal effects of genomic aberrations on gleason scores: A deep latent variable model. *Frontiers in oncology*, 10:272, 2020.

Dai, B., Wang, Z., and Wipf, D. The usual suspects? reassessing blame for vae posterior collapse. In *International Conference on Machine Learning*, pp. 2313–2322. PMLR, 2020.

He, J., Spokoyny, D., Neubig, G., and Berg-Kirkpatrick, T. Lagging inference networks and posterior collapse in variational autoencoders. *arXiv preprint arXiv:1901.05534*, 2019.

Hill, J. L. Bayesian nonparametric modeling for causal inference. *Journal of Computational and Graphical Statistics*, 20(1):217–240, 2011.

Jesson, A., Mindermann, S., Shalit, U., and Gal, Y. Identifying causal-effect inference failure with uncertainty-aware models. *Advances in Neural Information Processing Systems*, 33, 2020.

Kim, H., Shin, S., Jang, J., Song, K., Joo, W., Kang, W., and Moon, I.-C. Counterfactual fairness with disentangled causal effect variational autoencoder. *arXiv preprint arXiv:2011.11878*, 2020.

Kingma, D. P. and Welling, M. Auto-encoding variational bayes, 2013.

Kuroki, M. and Pearl, J. Measurement bias and effect restoration in causal inference. *Biometrika*, 101(2):423–437, 2014.

Louizos, C., Shalit, U., Mooij, J. M., Sontag, D., Zemel, R., and Welling, M. Causal effect inference with deep latent-variable models. In *Advances in Neural Information Processing Systems*, pp. 6446–6456, 2017.

Madras, D., Creager, E., Pitassi, T., and Zemel, R. Fairness through causal awareness: Learning causal latent-variable models for biased data. In *Proceedings of the Conference on Fairness, Accountability, and Transparency*, pp. 349–358, 2019.

Mayer, I., Josse, J., Raimundo, F., and Vert, J.-P. Missdeep-causal: Causal inference from incomplete data using deep latent variable models. *arXiv preprint arXiv:2002.10837*, 2020.

Miao, W., Geng, Z., and Tchetgen, E. T. Identifying causal effects with proxy variables of an unmeasured confounder, 2016.

Pawlowski, N., Coelho de Castro, D., and Glocker, B. Deep structural causal models for tractable counterfactual inference. *Advances in Neural Information Processing Systems*, 33, 2020.

Pearl, J. The seven tools of causal inference, with reflections on machine learning. *Communications of the ACM*, 62(3):54–60, 2019.

Pearl, J., Glymour, M., and Jewell, N. P. *Causal inference in statistics: A primer*. John Wiley & Sons, 2016.

Pfohl, S. R., Duan, T., Ding, D. Y., and Shah, N. H. Counterfactual reasoning for fair clinical risk prediction. In *Machine Learning for Healthcare Conference*, pp. 325–358. PMLR, 2019.

Rakesh, V., Guo, R., Moraffah, R., Agarwal, N., and Liu, H. Linked causal variational autoencoder for inferring paired spillover effects. In *Proceedings of the 27th ACM International Conference on Information and Knowledge Management*, pp. 1679–1682, 2018.

Razavi, A., Oord, A. v. d., Poole, B., and Vinyals, O. Preventing posterior collapse with delta-vae. *arXiv preprint arXiv:1901.03416*, 2019.

Rezende, D. J., Mohamed, S., and Wierstra, D. Stochastic backpropagation and approximate inference in deep generative models. In *International conference on machine learning*, pp. 1278–1286. PMLR, 2014.

Shalit, U., Johansson, F. D., and Sontag, D. Estimating individual treatment effect: generalization bounds and algorithms. In *International Conference on Machine Learning*, pp. 3076–3085, 2017.

Shi, C., Blei, D., and Veitch, V. Adapting neural networks for the estimation of treatment effects. In *Advances in Neural Information Processing Systems*, pp. 2507–2517, 2019.

Wang, Y. and Blei, D. M. The blessings of multiple causes. *Journal of the American Statistical Association*, 114(528): 1574–1596, 2019.

Yoon, J., Jordon, J., and van der Schaar, M. Ganite: Estimation of individualized treatment effects using generative adversarial nets. In *International Conference on Learning Representations*, 2018.

A. Analytical estimate of $p(y|do(t))$ for linear-Gaussian data

In this section, we derive an analytical estimate of the parameters of the $p(y|do(t))$ distribution for the linear-Gaussian data, including the ones that weren't provided in the original paper. It assumes that we know the parametric form of the generating process. The approach is slightly different from the original paper, which utilized higher-level properties of the structural model in their derivation. We will first derive the asymptotic, infinite data covariance matrix of the observed variables expressed using the data generating parameters $c_1, c_2, \sigma_1, \dots$, after which we can derive expressions for the parameters using observable covariances. The formulas can then be used as asymptotically correct estimates with finite data as well.

We start by finding out a form for the joint distribution, including z :

$$\begin{aligned} p(z, x, t, y) &= p(z)p(x|z)p(t|z)p(y|z, t) \\ &\sim e^{-\frac{1}{2} \left(z^2 + \frac{(c_1 z - x_1)^2}{\sigma_1^2} + \frac{(c_2 z - x_2)^2}{\sigma_2^2} + \frac{(c_t z - x_t)^2}{\sigma_t^2} + \frac{(c_{yz} z + c_{yt} t - y)^2}{\sigma_y^2} \right)} \end{aligned}$$

This is a jointly Gaussian distribution. We can find the covariance matrix by looking at the exponent and rearranging terms:

$$\begin{aligned} -2 \log p(z, x, t, y) &\sim z^2 \left(1 + \frac{c_1^2}{\sigma_1^2} + \frac{c_2^2}{\sigma_2^2} + \frac{c_t^2}{\sigma_t^2} + \frac{c_{yz}^2}{\sigma_y^2} \right) + zx_1 \left(-\frac{2c_1}{\sigma_1^2} \right) + \\ &\quad zx_2 \left(-\frac{2c_2}{\sigma_2^2} \right) + zt \left(-\frac{2c_t}{\sigma_t^2} + \frac{2c_{yz}c_{yt}}{\sigma_y^2} \right) + zy \left(-\frac{2c_{yz}}{\sigma_y^2} \right) + x_1^2 \frac{1}{\sigma_1^2} + \\ &\quad x_2^2 \frac{1}{\sigma_2^2} + t^2 \left(\frac{1}{\sigma_t^2} + \frac{c_{yt}^2}{\sigma_y^2} \right) + ty \left(-\frac{2c_{yt}}{\sigma_y^2} \right) + y^2 \left(\frac{1}{\sigma_y^2} \right) \\ &= [z \quad x_1 \quad x_2 \quad t \quad y] C^{-1} \begin{bmatrix} z \\ x_1 \\ x_2 \\ t \\ y \end{bmatrix} \end{aligned}$$

where

$$C^{-1} = \begin{bmatrix} 1 + \frac{c_1^2}{\sigma_1^2} + \frac{c_2^2}{\sigma_2^2} + \frac{c_t^2}{\sigma_t^2} + \frac{c_{yz}^2}{\sigma_y^2} & -\frac{c_1}{\sigma_1^2} & -\frac{c_2}{\sigma_2^2} & -\frac{c_t}{\sigma_t^2} + \frac{c_{yz}c_{yt}}{\sigma_y^2} & -\frac{c_{yz}}{\sigma_y^2} \\ -\frac{c_1}{\sigma_1^2} & \frac{1}{\sigma_1^2} & 0 & 0 & 0 \\ -\frac{c_2}{\sigma_2^2} & 0 & \frac{1}{\sigma_2^2} & 0 & 0 \\ -\frac{c_t}{\sigma_t^2} + \frac{2c_{yz}c_{yt}}{\sigma_y^2} & 0 & 0 & \frac{1}{\sigma_t^2} & -\frac{c_{yt}}{\sigma_y^2} \\ -\frac{c_{yz}}{\sigma_y^2} & 0 & 0 & -\frac{c_{yt}}{\sigma_y^2} & \frac{1}{\sigma_y^2} \end{bmatrix}$$

Inverting this, we get C , and the covariance matrix C_{xty} of the marginal distribution $p(x, t, y)$ is got by dropping the row and columns corresponding to z , since $p(z, x, t, y)$ is jointly Gaussian:

$$C_{xty} = \begin{bmatrix} c_1^2 + \sigma_1^2 & c_1 c_2 & c_1 c_t & c_1 (c_t c_{yt} + c_{yz}) \\ c_1 c_2 & c_2^2 + \sigma_2^2 & c_2 c_t & c_2 (c_t c_{yt} + c_{yz}) \\ c_1 c_t & c_2 c_t & c_t^2 + \sigma_t^2 & c_t^2 c_{yt} + c_t c_{yz} + c_{yt} \sigma_t^2 \\ c_1 (c_t c_{yt} + c_{yz}) & c_2 (c_t c_{yt} + c_{yz}) & c_t^2 c_{yt} + c_t c_{yz} + c_{yt} \sigma_t^2 & c_t^2 c_{yt}^2 + 2c_t c_{yt} c_{yz} + c_{yt}^2 \sigma_t^2 + c_{yz}^2 + \sigma_y^2 \end{bmatrix}$$

We then have a system of 10 equations, where each of the matrix cells corresponds to an asymptotic, infinite-data covariance. The equations of interest to us are

$$\begin{aligned} c_1 c_2 &= \text{Cov}(x_1, x_2), \quad c_1 c_t = \text{Cov}(x_1, t), \quad c_2 c_t = \text{Cov}(x_2, t), \quad c_t^2 + \sigma_t^2 = \text{Var}(t) \\ c_2 (c_t c_{yt} + c_{yz}) &= \text{Cov}(x_2, y), \quad c_t^2 c_{yt} + c_t c_{yz} + c_{yt} \sigma_t^2 = \text{Cov}(t, y) \\ c_t^2 c_{yt}^2 + 2c_t c_{yt} c_{yz} + c_{yt}^2 \sigma_t^2 + c_{yz}^2 + \sigma_y^2 &= \text{Var}(y) \end{aligned}$$

These can be solved to get

$$c_{yt} = \frac{\text{Cov}(t, y)\text{Cov}(x_1, x_2) - \text{Cov}(x_2, y)\text{Cov}(x_1, t)}{\text{Var}(t)\text{Cov}(x_1, x_2) - \text{Cov}(x_1, t)\text{Cov}(x_2, t)} \quad (6)$$

$$c_{yz}^2 = \frac{\text{Cov}(x_1, t)\text{Cov}(x_1, x_2)(\text{Cov}(t, y)\text{Cov}(x_2, t) - \text{Var}(t)\text{Cov}(x_2, y))^2}{\text{Cov}(x_2, t)(\text{Var}(t)\text{Cov}(x_1, x_2) - \text{Cov}(x_1, t)\text{Cov}(x_2, t))^2} \quad (7)$$

$$c_t^2 = \frac{\text{Var}(t)\text{Cov}(x_2, t)}{\text{Cov}(x_1, x_2)} \quad (8)$$

$$\sigma_t^2 = \text{Var}(t) - c_t^2 \quad (9)$$

$$c_t c_{yz} = \text{Cov}(t, y) - c_{yt} \sigma_t^2 - c_t^2 c_{yt} \quad (10)$$

$$\sigma_y^2 = \text{Var}(y) - c_{yz}^2 - c_{yt}^2 \sigma_t^2 - 2c_{yt} c_t c_{yz} - c_t^2 c_{yt}^2 \quad (11)$$

where earlier expressions can be plugged in to later ones (especially σ_y^2 doesn't simplify much). The quantities c_{yt} , c_{yz}^2 and σ_y^2 are enough to characterize $p(y|do(t))$, since

$$\begin{aligned} p(y|do(t)) &= \int_{-\infty}^{\infty} \frac{1}{\sqrt{2\pi}} e^{-\frac{z^2}{2}} \frac{1}{\sqrt{2\pi\sigma_y}} e^{-\frac{(y - c_{yz}z - c_{yt}t)^2}{2\sigma_y^2}} dz \\ &= \frac{1}{\sqrt{2\pi\sigma_{y|do(t)}}} e^{-\frac{(y - \mu_{y|do(t)})^2}{2\sigma_{y|do(t)}^2}} \end{aligned} \quad (12)$$

where

$$\mu_{y|do(t)} = c_{yt}t \quad (13)$$

$$\sigma_{y|do(t)} = \sqrt{\sigma_y^2 + c_{yz}^2} \quad (14)$$

In practice, we can use the asymptotically correct equations as formulas for estimation with finite data. The difference is that we use sample covariances and variances, and the parameter estimates are naturally correct only with infinite data.

B. Proof of Proposition 1: The 1D linear CEVAE identifies the correct causal effect with linear-Gaussian data

In section A we showed that the causal effect $p(y|do(t))$ is identifiable from linear-Gaussian data, and presented an asymptotically correct, analytical method for identification. Here we consider the 1D linear CEVAE, which estimates the conditional distributions linearly and has a latent dimension of one, thus being parameterized in the same way as the data generating process. We show that it is guaranteed to get the correct causal effect as well, assuming that we find the global optimum of the ELBO with infinite data. The proof relies on three facts:

1. As shown in Sec.A, the parameters of the data generating process required for identifying the causal effect match one-to-one with observed covariances.
2. The CEVAE estimation model is defined so that the parameters match exactly with the data generating parameters and the prior is correctly specified as well.
3. The variational approximation to the posterior distribution can correctly represent the true posterior in this case.

Proof. We denote $p_\theta(\cdot)$ as the distribution induced by the VAE, e.g. $p_\theta(z, x, t, y) = p_\theta(x_1|z)p_\theta(x_2|z)p_\theta(t|z)p_\theta(y|z, t)p(z)$, where $p(z)$ is the zero mean, unit variance prior of the VAE.

Since the joint distribution $p_\theta(z, x, t, y)$ induced by the model is jointly Gaussian with mean zero, we know from properties of multivariate normal distributions that $p_\theta(z|x, t, y)$ is Gaussian as well with a mean that is a linear function of x_1, x_2, t and y with zero bias and constant variance. Thus, as we set our variational approximation $q_\phi(z|x, t, y)$ to be similarly a Gaussian with mean being a linear function of the observed variables and estimate the variance as one shared parameter, it can represent the true posterior $p_\theta(z|x, t, y)$ with the right choice of parameters ϕ . Thus, the global optimum of the ELBO

also equals the global optimum of the marginal log-likelihood. In the limit of infinite data, maximizing the sum of marginal log-likelihoods becomes equivalent to maximizing

$$\begin{aligned} \int p(x, t, y) \log p_\theta(x, t, y) dz &= \int p(x, t, y) \log \left(\frac{p_\theta(x, t, y)}{p(x, t, y)} p(x, t, y) \right) dx dt dy \\ &= -KL[p(x, t, y) || p_\theta(x, t, y)] + \int p(x, t, y) \log p(x, t, y) dx dt dy \end{aligned} \quad (15)$$

where $p(x, t, y)$ is the true distribution of the data. Thus, since the parameter space of the linear VAE includes the true distribution, at the globally optimal (θ, ϕ) combination the KL divergence goes to zero and $p_\theta(x, t, y) = p(x, t, y)$, i.e., the marginal distribution of our model is the true distribution. Because the VAE parameterization was defined in the exact same way as the generative model, we can then go through the exact same steps as we did in Sec. A, and notice that the estimate of $p(y|do(t))$ has to be the one we get from the true distribution. Thus, the model identifies $p(y|do(t))$ correctly. \square

C. Proof of Proposition 2: We can get an infinite ELBO with copied proxies

In this section, we prove that we can get an infinite ELBO by using the latent space solely to reconstruct the proxies for linear-Gaussian data where the proxies are copied at least once. The proof assumes a linear CEVAE estimation model with a latent dimension of at least two, but the result is valid for a neural network parameterized CEVAE as well assuming that it can represent the same conditional distributions as the linear CEVAE. Given the universal approximation capabilities of neural networks, this is not a very radical assumption to make. The central idea in the proof is that we find a certain path in the parameter space which we then show to lead to an infinite evidence lower bound. It is constructed by mapping each value of x to a corresponding position in the latent space, after which we let the encoder and decoder variances go to zero, forcing the reconstruction to become perfect.

Proof. Recall that the ELBO for CEVAE can be written in the form

$$\begin{aligned} \mathcal{L}(\theta, \phi) &= \sum_i [\mathbb{E}_{q_\phi(z|x^i, t^i, y^i)} [\log p_\theta(x^i|z) + \log p_\theta(t^i|z) + \log p_\theta(y^i|z, t^i)] - \\ &\quad KL[q_\phi(z|x^i, t^i, y^i) || p(z)]] \end{aligned} \quad (16)$$

Let us now consider the scenario where we are trying to estimate the causal effect from a data set containing N copies of the original two proxies. We restrict the analysis to the part of the parameter space where the variational approximation depends only on the proxies and both proxies are reconstructed using only one of the dimensions:

$$q_\phi(z|x, t, y) = \mathcal{N}(z|\mu_{z|x}, S_{z|x}) \quad (17)$$

$$\mu_{z|x} = \begin{bmatrix} \gamma_{z_1} x_1 \\ \gamma_{z_2} x_2 \end{bmatrix} \quad (18)$$

$$S_{z|x} = \begin{bmatrix} s_{z_1|x}^2 & 0 \\ 0 & s_{z_2|x}^2 \end{bmatrix} \quad (19)$$

The proxy distribution in the decoder is set to $p_\theta(\{x_i\}|z) = \mathcal{N}(x_i|\gamma_i z, s_i^2)^N$, where γ_i and s_i are shared parameters for x_i and all its copies, denoted by the set $\{x_i\}$ and N is the number of copies $|\{x_i\}|$. Note that we use γ and s to highlight that these are parameters of CEVAE, not the data generating distribution, where we used c and σ . Let's focus on the proxy reconstruction term and the KL divergence terms for the first latent dimension - proxy copy group pair, z_1 and $\{x_1\}$. The reconstruction term for a single observation is

$$\mathbb{E}_{q_\phi(z_1|x, t, y)} [\log p_\theta(\{x_1\}|z)] = \int \frac{1}{\sqrt{2\pi s_{z_1|x}}} \exp\left(-\frac{(z_1 - \gamma_{z_1} x_1)^2}{2s_{z_1|x}^2}\right) \log \left[\left(\frac{1}{\sqrt{2\pi s_1}} \exp\left(-\frac{(x_1 - \gamma_1 z)^2}{2s_1^2}\right) \right)^N \right] dz \quad (20)$$

$$= \int \frac{1}{\sqrt{2\pi s_{z_1|x}}} \exp\left(-\frac{(z_1 - \gamma_{z_1} x_1)^2}{2s_{z_1|x}^2}\right) N \left(\log \frac{1}{\sqrt{2\pi s_1}} - \frac{(x_1 - \gamma_1 z)^2}{2s_1^2} \right) dz \quad (21)$$

$$= N \log \frac{1}{\sqrt{2\pi s_1}} - N \frac{\sqrt{s_{z_1}}}{2s_1^2} (\gamma_1^2 s_{z_1}^2 + x_1^2 (1 - \gamma_1 \gamma_{z_1})) \quad (22)$$

where the exponentiation by N is due to the N identical copies that are reconstructed using the same parameters. Due to the diagonal assumptions in the prior and variational approximation, the KL divergence breaks into two parts:

$$-KL[q_\phi(z|x_1, \{x_2\}, t, y) || p(z_1)]$$

$$= - \int \int \mathcal{N}(z_1|\gamma_{z_1}x_1, s_{z_1|x}^2) \mathcal{N}(z_2|\gamma_{z_2}x_2, s_{z_2|x}^2) \log \left(\frac{p(z_1)p(z_2)}{\mathcal{N}(z_1|\gamma_{z_1}x_1, s_{z_1|x}^2) \mathcal{N}(z_2|\gamma_{z_2}x_2, s_{z_2|x}^2)} \right) dz_1 dz_2 \quad (23)$$

$$= -KL[\mathcal{N}(z_1|\gamma_{z_1}x_1, s_{z_1|x}^2) || p(z_1)] - KL[\mathcal{N}(z_2|\gamma_{z_2}x_2, s_{z_2|x}^2) || p(z_2)] \quad (24)$$

where the term relevant for parameters regarding z_1 and x_1 is

$$-KL[\mathcal{N}(z_1|\gamma_{z_1}x_1, s_{z_1|x}^2) || p(z_1)] = -\log \frac{1}{s_{z_1|x}} - \frac{s_{z_1|x}^2 + \gamma_{z_1}x_1^2}{2} + \frac{1}{2} \quad (25)$$

Bringing the two terms together and restricting the parameter space further so that $\gamma_1\gamma_{z_1} = 1$ and $s_1^{\frac{4}{5}} = s_{z_1|x} = s$, we have

$$\begin{aligned} \mathbb{E}_{q_\phi(z_1|x, t, y)}[\log p_\theta(x_1|z)] - KL[\mathcal{N}(z_1|\gamma_{z_1}x_1, s_{z_1|x}^2) || p(z_1)] \\ = N \log \frac{1}{\sqrt{2\pi}s_1} - N \frac{\sqrt{s_{z_1}}}{2s_1^2} (\gamma_1^2 s_{z_1}^2 + x_1^2(1 - \gamma_1\gamma_{z_1})) - \log \frac{1}{s_{z_1|x}} - \frac{s_{z_1|x}^2 + \gamma_{z_1}x_1^2}{2} + \frac{1}{2} \end{aligned} \quad (26)$$

$$= -\frac{5N}{8} \log s - N \frac{\gamma_1^2}{2} + \log s - \frac{s^2}{2} + \text{constants} \quad (27)$$

Let's now consider the two scenarios where $N = 1$ and $N = 2$ we let $s \rightarrow 0$.

N=1 The sum of the relevant, non-constant terms in the limit approaches minus infinity:

$$\lim_{s \rightarrow 0} \left(-\frac{5}{8} \log s - \frac{\gamma_1^2}{2} + \log s - \frac{s^2}{2} \right) = \lim_{s \rightarrow 0} \left(\frac{3}{8} \log s \right) + 0 = -\infty \quad (28)$$

Thus, with no copies this approach clearly doesn't maximize the ELBO.

N=2 The sum approaches infinity in the limit:

$$\lim_{s \rightarrow 0} \left(-\frac{10}{8} \log s - \gamma_1^2 + \log s - \frac{s^2}{2} \right) = \lim_{s \rightarrow 0} \left(-\frac{1}{4} \log s \right) + 0 = +\infty \quad (29)$$

Although we only focused on a single observation in the ELBO, the final expression is not actually dependent on the values of x_1 , so the ELBO will go to infinity for all observations with this parameterization. We can do the exact same thing for the second group of proxies $\{x_2\}$ and the second latent variable z_2 . We conclude that while exactly this approach might not be the fastest way to increase the ELBO during training, it is clearly possible to get an infinite ELBO by using the latent space solely to reconstruct the proxies as accurately as possible. \square

In practice, the model could then follow a similar path as a result of gradient descent during training. Figure 6 shows the ELBO and its parts for a full, neural network parameterized CEVAE with copied proxies. While t and y reconstruction terms in the ELBO converge very early, the x reconstruction term keeps improving long after that. The negative KL divergence term gets smaller, but it is not enough to counter the increase in x reconstruction quality.

Intuitively, the reason that the final expression doesn't depend on the values of observed x is that the latent space is able to represent the proxies perfectly, i.e., each x_1 is mapped to a corresponding latent representation through the γ_{z_1} parameter. We restricted $\gamma_1\gamma_{z_1} = 1$ because if the latent representation of the proxy was scaled down or up by γ_{z_1} , we need to do the opposite scaling $\gamma_1 = \frac{1}{\gamma_{z_1}}$ in reconstruction.

Note that if the latent dimension is larger than two, we won't improve the ELBO by using them to reconstruct the treatment t and effect y , as shown in Sec.D. Thus, the $p_\theta(t|z)$ and $p_\theta(y|z, t)$ reconstruction terms may only improve if the proxies, through the latent representation, are useful for predicting y and t .

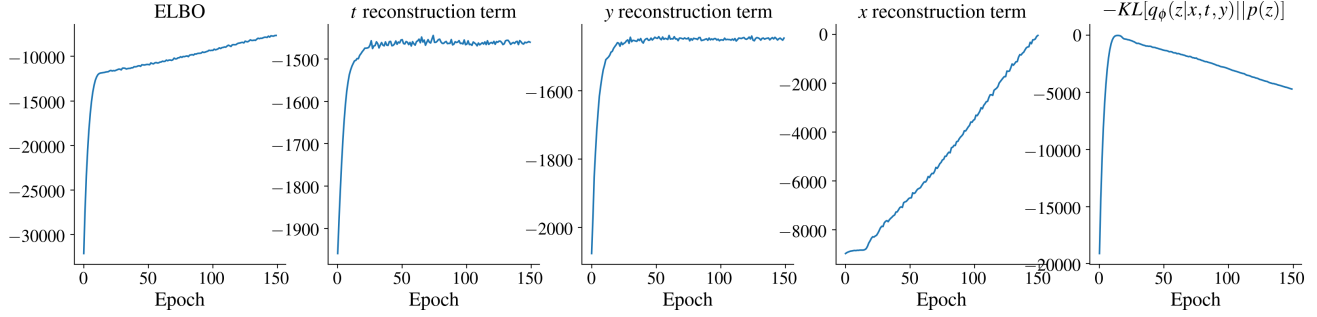


Figure 6. The ELBO and its parts for the linear-Gaussian data with exact proxies. The estimation model was the full, NN parameterized CEVAE. The data generating process was the same as in the main experiment, but without additional noise on the copies. The sample size was set to 1000, batch size was 200 and learning rate was 0.0001.

D. Proof of Proposition 3: Posterior collapse in the 1D linear CEVAE with no proxies

Here we show analytically that if the proxy reconstruction term is set to zero (essentially, we don't have any proxies), the posterior collapsed solution where we ignore all confounding is a global maximum of the ELBO with linear-Gaussian data. Additionally, the causal effect estimate $p_\theta(y|do(t))$ will equal to $p(y|t)$. In the proof, we assume that the estimation model is the CEVAE with a one-dimensional latent space and linearly parameterized conditionals. However, the result applies to a CEVAE with neural network parameterization as well if we assume that it is able to represent the same conditionals as the linear CEVAE.

Proof. Let's assume that we have maximized the ELBO so that $q_\phi(z|x, t, y) = p_\theta(z|t, y)$ for whatever θ that can maximize it. Then, with infinite data, according to Eq.15, we get that $p(t, y) = p_\theta(t, y)$. Let us use the notation γ and s to signify the CEVAE parameters that correspond to the parameters c and σ in the data generating model. In a similar way as in Sec.A we can then show that the inverse of the covariance matrix of $p_\theta(z, t, y)$ is then

$$C^{-1} = \begin{bmatrix} 1 + \frac{\gamma_t^2}{s_t^2} + \frac{\gamma_{yz}^2}{s_y^2} & -\frac{\gamma_t}{s_t^2} + \frac{\gamma_{yz}\gamma_{yt}}{s_y^2} & -\frac{\gamma_{yz}}{s_y^2} \\ -\frac{\gamma_t}{s_t^2} + \frac{\gamma_{yz}\gamma_{yt}}{s_y^2} & \frac{1}{s_t^2} & -\frac{\gamma_{yt}}{s_y^2} \\ -\frac{\gamma_{yz}}{s_y^2} & -\frac{\gamma_{yt}}{s_y^2} & \frac{1}{s_y^2} \end{bmatrix}$$

Inverting and marginalizing w.r.t. z , we then get

$$C_{ty} = \begin{bmatrix} \gamma_t^2 + s_t^2 & \gamma_t^2\gamma_{yt} + \gamma_t\gamma_{yz} + \gamma_{yt}s_t^2 \\ \gamma_t^2\gamma_{yt} + \gamma_t\gamma_{yz} + \gamma_{yt}s_t^2 & \gamma_t^2\gamma_{yt}^2 + 2\gamma_t\gamma_{yt}\gamma_{yz} + \gamma_{yt}^2s_t^2 + \gamma_{yz}^2 + s_y^2 \end{bmatrix}$$

We have the equations

$$\begin{aligned} \text{Var}(t) &= \gamma_t^2 + s_t^2 \\ \text{Var}(y) &= \gamma_t^2\gamma_{yt}^2 + 2\gamma_t\gamma_{yt}\gamma_{yz} + \gamma_{yt}^2s_t^2 + \gamma_{yz}^2 + s_y^2 \\ \text{Cov}(t, y) &= \gamma_t^2\gamma_{yt} + \gamma_t\gamma_{yz} + \gamma_{yt}s_t^2 \end{aligned}$$

This group of equations has more than one solution, but an obvious one is $\gamma_t = 0, \gamma_{yz} = 0, s_t^2 = \text{Var}(t), s_y^2 = \text{Var}(y) - \text{Cov}(t, y)$ and $\gamma_{yt} = \frac{\text{Cov}(t, y)}{\text{Var}(t)^2}$. This corresponds to the solution where we ignore the latent space entirely and the posterior approximation equals the prior. We can also show that $p_\theta(y|do(t)) = p(y|t)$, by first calculating $p_\theta(y|do(t))$:

$$\begin{aligned} p_\theta(y|do(t)) &= \int p_\theta(y|z, t)p(z)dz \\ &= p_\theta(y|t) \\ &= \mathcal{N}(y|\gamma_{yt}t, s_y^2) = \mathcal{N}(y|\frac{\text{Cov}(t, y)}{\text{Var}(t)^2}t, \text{Var}(y) - \text{Cov}(t, y)) \end{aligned} \tag{30}$$

Here the second equality is true because y is not dependent on z . The result corresponds to the conditional distribution formula for bivariate Gaussians: $p(y|t) = \mathcal{N}(y | \frac{\text{Cov}(t,y)}{\text{Var}(t)} t, \text{Var}(y) - \text{Cov}(t,y))$. \square

Other solutions to the group of equations are possible in principle, but in practise the training usually converges to this posterior collapsed solution, as witnessed in the experiments. Note that while the proof applies strictly speaking only to the 1D linear CEVAE, the result is true for a neural-network parameterized CEVAE as well if it is able to represent the same conditional distributions. The solution is a global optimum with both parameterizations since already $p_\theta(t, y) = p(t, y)$, and thus it's not possible to improve the ELBO according to Eq.15.

E. Experiment details

E.1. Computing equipment, time taken to run experiments and code

The experiments were performed with two computers: A desktop computer containing an Intel i5-6500 processor and an Nvidia GTX 970 graphics card, and a laptop containing an AMD A12-9720P processor. Most of the experiments E.2-E.7 in this section took at most a single night to run with the computing equipment, although the binary data experiment took approximately an entire day. The basic Linear-Gaussian and binary experiments were conducted with the laptop, while the others were done with the desktop computer. The graphics card was used for the proxy MNIST data set, while the processor of the desktop was used for the rest.

The code for running the experiments is at https://github.com/skwfz/critical_look_causal_dlvms

E.2. Linear-Gaussian data

Data generating parameters The generating parameters were sampled with the following process: First, all of the standard deviations σ were generated from a $\text{Gamma}(1,5)$ distribution. Then, the structural coefficients c were got by first sampling from a $\text{Gamma}(0.3,4)$ distribution, multiplying with the corresponding σ and adding the result to $\sigma/2$, and uniformly randomly flipping to a negative value. This resulted in the ratio $\frac{c}{\sigma}$ being not too close to zero while keeping the absolute values of σ and c roughly in the scale of 1. Too low a ratio for proxy, for instance, would mean that the proxy would be effectively very uninformative, and could cause even the analytical methods to fail. The generated parameters for the main experiment were $c_1 = 1.03$, $c_2 = 1.47$, $c_{yz} = 0.71$, $c_{yt} = -0.62$, $\sigma_{x_1} = 0.65$, $\sigma_{x_2} = 0.96$, $\sigma_t = 1.25$ and $\sigma_y = 0.48$.

Estimation models The default setup for the full, neural network parameterized CEVAE was so that each conditional distribution was represented with a three-layer MLP with a layer width of 30, using ELU activations. The (standard) assumption in the parameterization was that the outputs are normally distributed with a diagonal covariance for each network in the encoder and decoder. Thus, the final layers had twice the amount of heads than the output dimension, one for each mean and one for each standard deviation. There were four networks: The encoder, the proxy generation network ($p_\theta(x|z)$), the t generation network ($p_\theta(t|z)$) and the y generation network ($p_\theta(y|z, t)$). The dimension of the latent space was 10 for the default model. In the linear versions of CEVAE, the conditional distributions were defined with simple linear layers, and the standard deviations were separate, shared parameters used for all inputs.

Training The Adam optimizer was used for all models in this work. The neural network-based models were trained with 300 epochs, as that provided good loss function convergence for all data sizes. For the linear models, we used 500 epochs. The learning rates were annealed exponentially from 0.01 to 0.001. The batch size was 200. 10 data sets were sampled for each data size, and the models were trained once for each data set. The results from training to them provide the box plots in the results.

Posterior collapse Figure 7 visualizes the posterior collapse phenomenon for the 10 models trained with a data size of 20000. It shows the squared expected values $\mathbb{E}[q_\phi(z|x, t, y)]^2$ for each of the 10 dimensions, averaged over the data set (in other words, the variances of the encoder means for the data set). We see that all of the models use only one of the latent dimensions, while all the unused dimensions in the posterior approximation fall back to the mean of the prior.

Failed 2D estimation In the linear, 2D CEVAE experiment with failed estimation, we tried to initialize the model so that the parameters included aspects of the "correct" parameters, but were also sufficiently different to lead the model to incorrect estimation after training. The chosen initialization was also not itself a minimum of the loss function. Figure 8a shows the initialization. We tried to be very careful with the training by increasing the batch size to 1000, setting the learning rate to 0.001 and training until the model appeared to converge. In Fig.8b-c we plot the losses and estimates for the c_{yt} coefficients

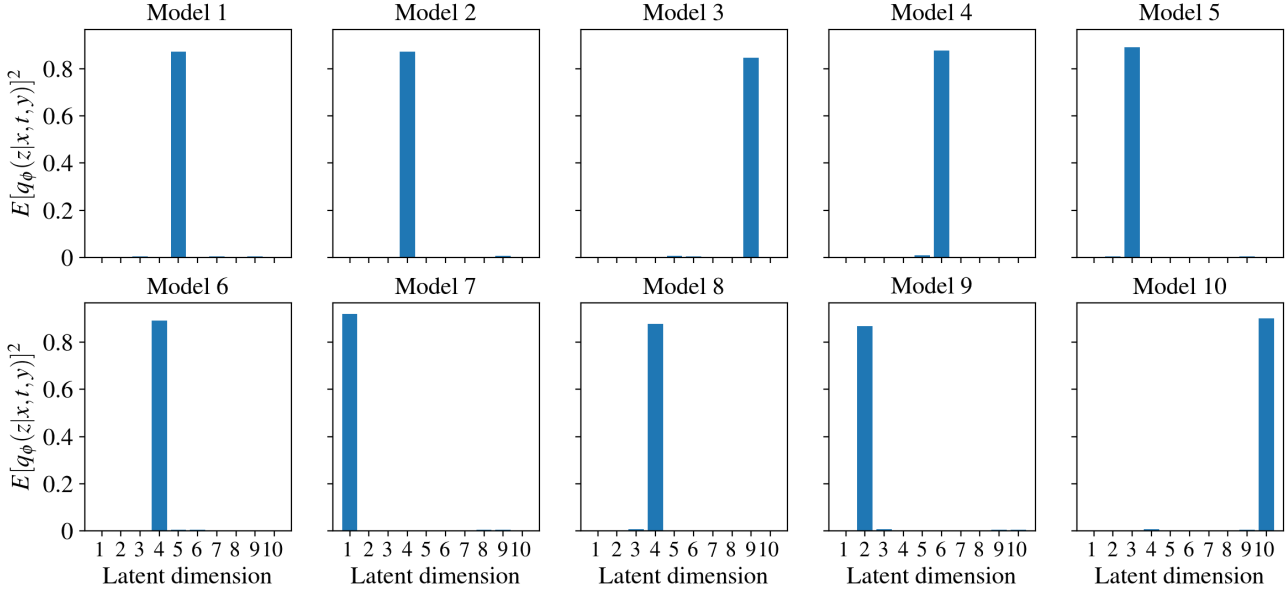


Figure 7. The squared expected values of the posterior approximations for the full 10D CEVAE with linear-Gaussian data, averaged over their respective data sets. Each of the models was trained on one of the linear-Gaussian data sets of size 20000.

as the training progressed. While the custom initialization results in an indistinguishable loss, the resulting causal effect is clearly wrong.

E.3. Binary data

Data generating parameters The data generating parameters were generated from a Dirichlet(2) distribution for the prior $p(z)$ as well as all the conditional distributions. The distribution was chosen so that probabilities close to 0 or 1 would be unlikely, as too high or low probabilities can result in a pathological case where the data is very difficult to estimate from. The parameters for the main experiment were $p(z = 1) = 0.56$, $p(x_1 = 1|z = 0) = 0.56$, $p(x_1 = 1|z = 1) = 0.73$, $p(x_2 = 1|z = 0) = 0.94$, $p(x_2 = 1|z = 1) = 0.26$, $p(t = 1|z = 0) = 0.71$, $p(t = 1|z = 1) = 0.16$, $p(y = 1|z = 0, t = 0) = 0.57$, $p(y = 1|z = 0, t = 1) = 0.36$, $p(y = 1|z = 1, t = 0) = 0.17$ and $p(y = 1|z = 1, t = 1) = 0.04$.

Estimation models The default setup for the full CEVAE was the same as in the Linear-Gaussian experiment, except that the neural network heads for the decoder were transformed through logistic link functions to probabilities, and the output was interpreted as a standard Bernoulli distribution. We also tried a model with a binary latent space, which was otherwise the same as the regular model, except the encoder had just one head, and the output was similarly interpreted as a Bernoulli distributed variable. The probability parameter of the Bernoulli distributed prior $p(z)$ was included as a learnable parameter. The expectation $\mathbb{E}_{q_\phi(z_i|x_i, t_i, y_i)}[\log p_\theta(x_i, t_i, y_i|z)]$ was calculated directly by passing both values of z through the decoder weighting the log probabilities with $q_\phi(z_i|x_i, t_i, y_i)$.

Training The models were trained for 300 epochs with the Adam optimizer, with learning rate annealing from 0.01 to 0.0005, as that seemed to produce good loss function convergence. 10 data sets were sampled for each data size, and the batch size was 200.

Binary CEVAE results

Figure 9 shows the results from the binary CEVAE. It performs very well, and the causal effect estimates become better as the sample size is increased. However, the model doesn't work as well for all data generating processes, such as some of the ones in Sec. F.2, where it seemed that the model can get stuck in local minima easily.

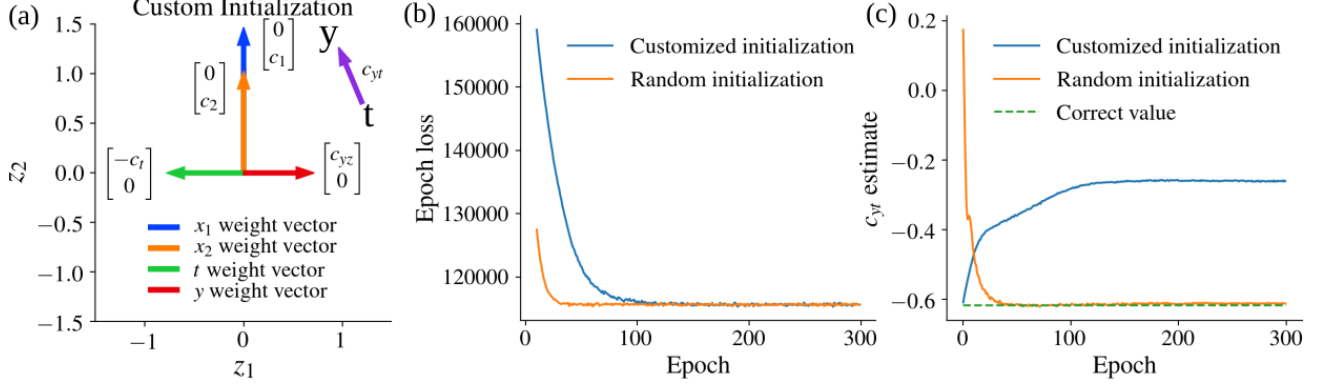


Figure 8. (a) Custom initialization of the 2D linear CEVAE that results in the wrong causal effect. The variances were set to the correct values and the posterior approximation was set so that it was the true posterior given the initialized decoder parameters. (b) Epoch losses of the custom initialized CEVAE and a successful, randomly initialized 2D linear CEVAE for comparison. (b) Estimates of c_{yt} , taken as the coefficient of t in the linear predictor for $y|z, t$ in the decoder.

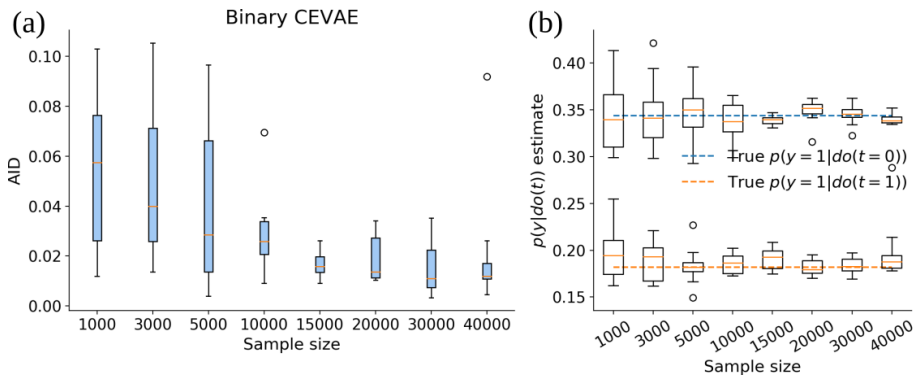


Figure 9. The AID and $p(y|do(t))$ estimates as a function of sample size for the binary CEVAE and binary data.

E.4. Linear-Gaussian data with redundant noise

Data generation The parameters for the first phase of the data generating distribution were $c_1 = 1$, $c_2 = 2$, $c_t = 0.5$, $c_{yz} = 0.6$, $c_{yt} = 1$, $\sigma_1 = 0.5$, $\sigma_2 = 0.7$, $\sigma_3 = 20$, $\sigma_t = 1$ and $\sigma_y = 1$ (c_3 was 0). After generating data from the linear-Gaussian distribution defined with these parameters, an additional orthogonal transformation was applied on the proxies so that the matrix was

$$R = \begin{bmatrix} \cos \alpha & -\sin \alpha & 0 \\ \sin \alpha & \cos \alpha & 0 \\ 0 & 0 & 1 \end{bmatrix} \begin{bmatrix} \cos \beta & 0 & \sin \beta \\ 0 & 1 & 0 \\ -\sin \beta & 0 & \cos \beta \end{bmatrix} \begin{bmatrix} 1 & 0 & 0 \\ 0 & \cos \gamma & -\sin \gamma \\ 0 & \sin \gamma & \cos \gamma \end{bmatrix} \quad (31)$$

where $\alpha = \frac{\pi}{4}$, $\beta = \frac{\pi}{4}$ and $\gamma = \frac{\pi}{4}$. Here α , β and γ are also called the yaw, pitch and roll angles in the 3D space.

Estimation models and training The parameters of CEVAE and training were otherwise identical to the full CEVAE linear-Gaussian experiment, but the latent space was changed to one-dimensional and two-dimensional for the two setups explained in the main text.

E.5. Linear-Gaussian data with copied proxies

Data generation The data generating parameters were $c_1 = 1$, $c_2 = 1$, $c_t = 0.5$, $c_{yz} = 0.6$, $c_{yt} = 1$, $\sigma_1 = 2$, $\sigma_2 = 2$, $\sigma_t = 1$ and $\sigma_y = 1$. \tilde{x}_1 and \tilde{x}_2 were copies of x_1 and x_2 , with Gaussian noise of standard deviation 0.1 added.

Estimation model Other experimental parameters were exactly the same as for the full CEVAE in the linear-Gaussian experiment, except that we used a linear predictor for y to make the results easier to interpret.

Training Training took only 100 epochs when trying out different loss scaling values, since that was clearly enough for convergence. The sample size was 20000 for the loss scaling experiment.

E.6. Proxy IHDP data

Data generation The data generating VAE was defined so that the encoder and decoder were MLPs with 3 layers and layer width 30 and a latent dimension of 10. The decoder was structured with the assumption that continuous variables had a Gaussian distribution at the outputs of the neural networks and categorical variables were categorically distributed with a softmax layer or logistic link function at the end for binary variables. The fourth variable in the IHDP data set was transformed to categorical since only four distinct values occurred in the data set. Variances were estimated individually for each sample for the continuous variables with the neural networks. We chose the fifth variable as the unobserved confounder, and left the rest as the proxies. ATE was set to 1 and the added Gaussian noise on y had a standard deviation of 1. Figure 10 presents some aspects of the generating process: The chosen unobserved confounder is approximately normally distributed and it is clearly correlated with many of the observed variables. Panel (c) also visualizes the dependence of t on z .

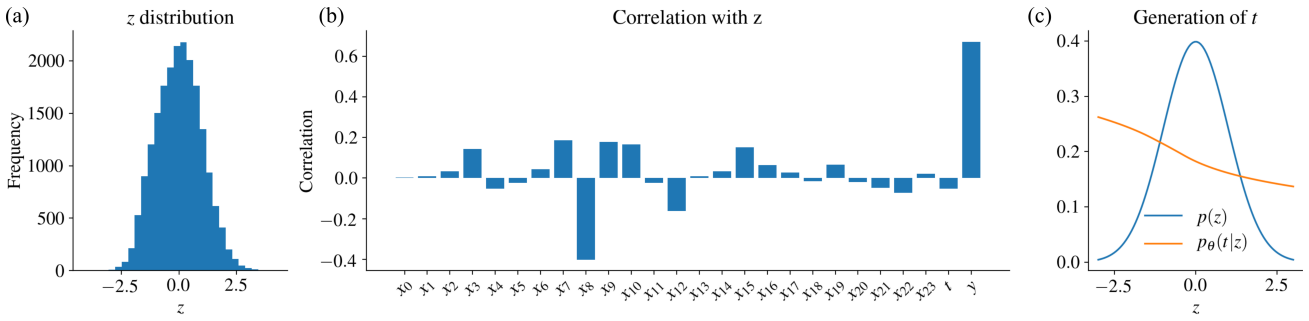


Figure 10. Properties of the IHDP data generating process. (a) The distribution of the chosen unobserved confounder. (b) Correlation of the chosen z with the proxies, t and y . (c) Visualization of the $p(t|z)$ function in the data generating process.

Estimation model The CEVAE model used for the data was defined similarly as the data generating VAE, with the addition of t and y prediction networks in the decoder. Another difference was that there were two separate networks in the decoder for y generation that were chosen based on the value of t on each pass. Likewise, the encoder consisted of four parallel networks that were chosen based on the value combination of t and y for each sample. The aim was to force the model to

take t and y in to account in the reconstruction process, in a similar way as in the original CEVAE publication. Also, the fifth variable in the IHDP data naturally wasn't included in the proxies.

Training Training was done for 200 epochs with a batch size of 200 and exponential learning rate annealing from 0.001 to 0.00001. The sample size for the loss scaling experiment was 20000.

Additional results Figure 11 shows the experimental results for $p(y = 1|do(t = 0))$. We see that the conclusions are the same as for $p(y = 1|do(t = 1))$, which was presented in the main text.

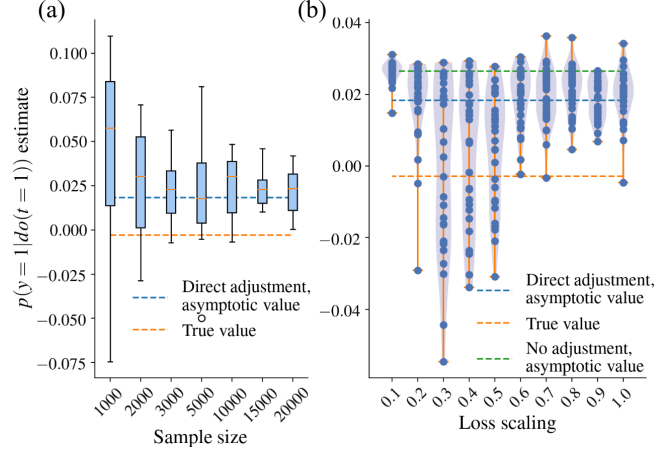


Figure 11. The $p(y = 1|do(t = 0))$ estimates with respect to sample size and loss scaling with sample size set to 20000.

E.7. Proxy MNIST data

Data generation The data generating GAN had a simple four-layer convolutional architecture in the discriminator and similarly four transpose convolutional layers in the generator. The exact details are in the code accompanying the article.

Estimation model The CEVAE model had was structured in a similar way as the GAN, with four transpose convolutional layers in the image part of the decoder. The other neural networks for the extra linear-Gaussian proxy, t and y were three-layer MLPs of width 30. Two NNs were defined for y , chosen depending on the value of t , the attempt being to define the conditional distributions as well as possible for the task. The encoder consisted of three parts. First, we had the four transpose convolutional layers starting from the images and ending up with 40 outputs. Second, we had a set of four fully connected linear layers with the 40 previous outputs and the additional proxy variable as inputs, with an output size of 125. One of the four networks was then chosen on each pass based on the value combination of t and y . The third part was similarly a set of 4 fully connected linear layers with input size 25 and output size 40, where one of the networks was again chosen based on the values of t and y . Again, the aim was to force the encoder to take t and y in to account. The final output was used to define the means and variances of the variational approximation in the 20-dimensional latent space. The convolutional and transpose convolutional layers were different from the corresponding GAN layers in that some of the kernel sizes, strides and paddings were changed around just so that the estimation model didn't match exactly with the data generation model.

Training The models were trained for 500 epochs (as shown in the Figures in the main text) with a batch size of 1000 and exponential schedule learning rate annealing from 0.003 to 0.001.

F. Replicated experiments

F.1. Linear-Gaussian data

We sampled four other data generating distributions with the process detailed in Section E.2 and ran the same experiment comparing the convergence of AID values on each process. The parameters are presented in Table 1. Figure 12 shows the results. While the convergence of AID values to zero happens differently for different data generating processes, the main conclusion stays the same. The estimates of the full CEVAE model are usually slightly less accurate than the 1D linear CEVAE and the analytical method, but they do steadily improve as the sample size increases.

Table 1. Data generating parameters for the repeated linear-Gaussian experiments.

	c_1	c_2	c_t	c_{yz}	c_{yt}	σ_1	σ_2	σ_t	σ_y
Process 1	-0.53	0.92	0.99	-1.15	0.46	0.71	1.02	1.14	0.84
Process 2	1.05	-0.57	-0.83	0.76	-1.38	1.04	0.77	0.68	1.11
Process 3	1.30	-1.02	0.80	1.17	1.11	1.02	0.91	1.27	0.88
Process 4	-1.58	0.80	-0.82	0.99	-1.13	1.28	0.87	1.04	0.77

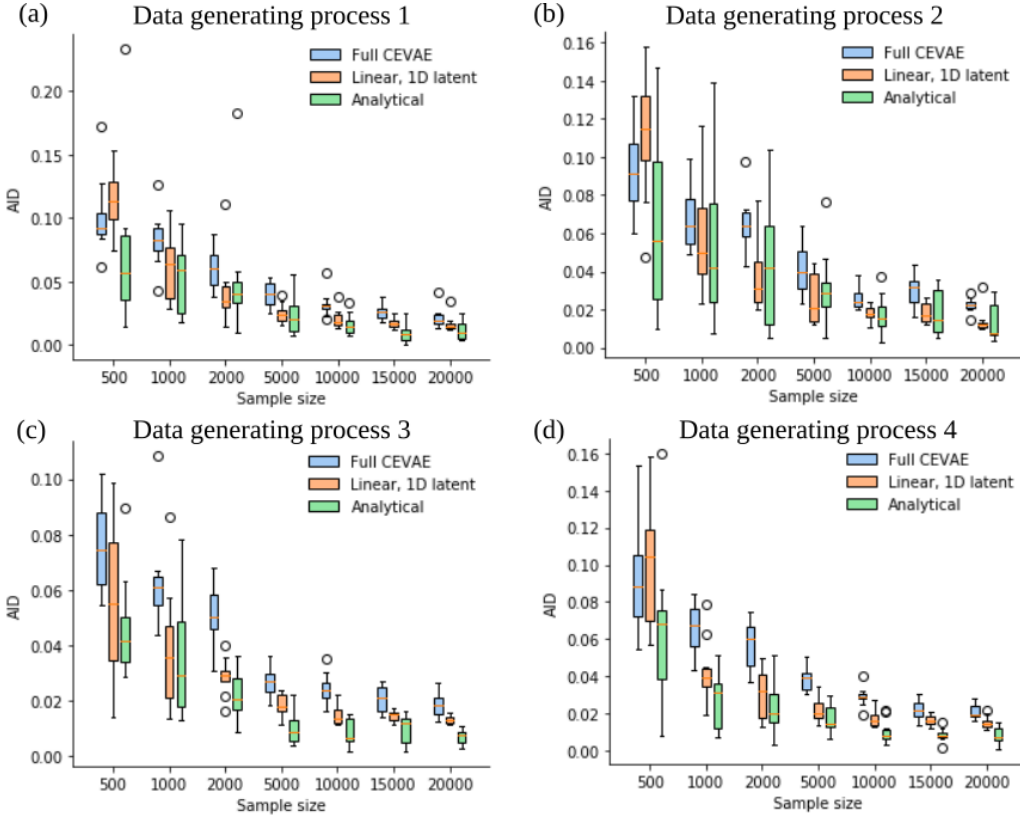


Figure 12. The AID values with respect to sample size for the replicated linear-Gaussian experiments.

F.2. Binary data

Four other data generating processes were sampled from the distribution explained in Sec.E.3, and the same experiment as in the main text was run for each data generating process. The results are presented in Fig.13. Aside from possibly the second data set, CEVAE consistently estimates the causal effects incorrectly. The analytical method is not very accurate with small sample sizes, but the average estimate is correct, in contrast to CEVAE. The fact that CEVAE performed well especially on the second data generating process may be due to the true causal effects being very close to the effects we get without adjustment at all (compare $p(y = 1|do(t = 0)) = 0.468$ to $p(y = 1|t = 0) = 0.473$ and $p(y = 1|do(t = 1)) = 0.138$ to $p(y = 1|t = 1) = 0.136$). The parameters of the data generating processes are detailed in table 2.

A Critical Look at the Identifiability of Causal Effects with Deep Latent Variable Models

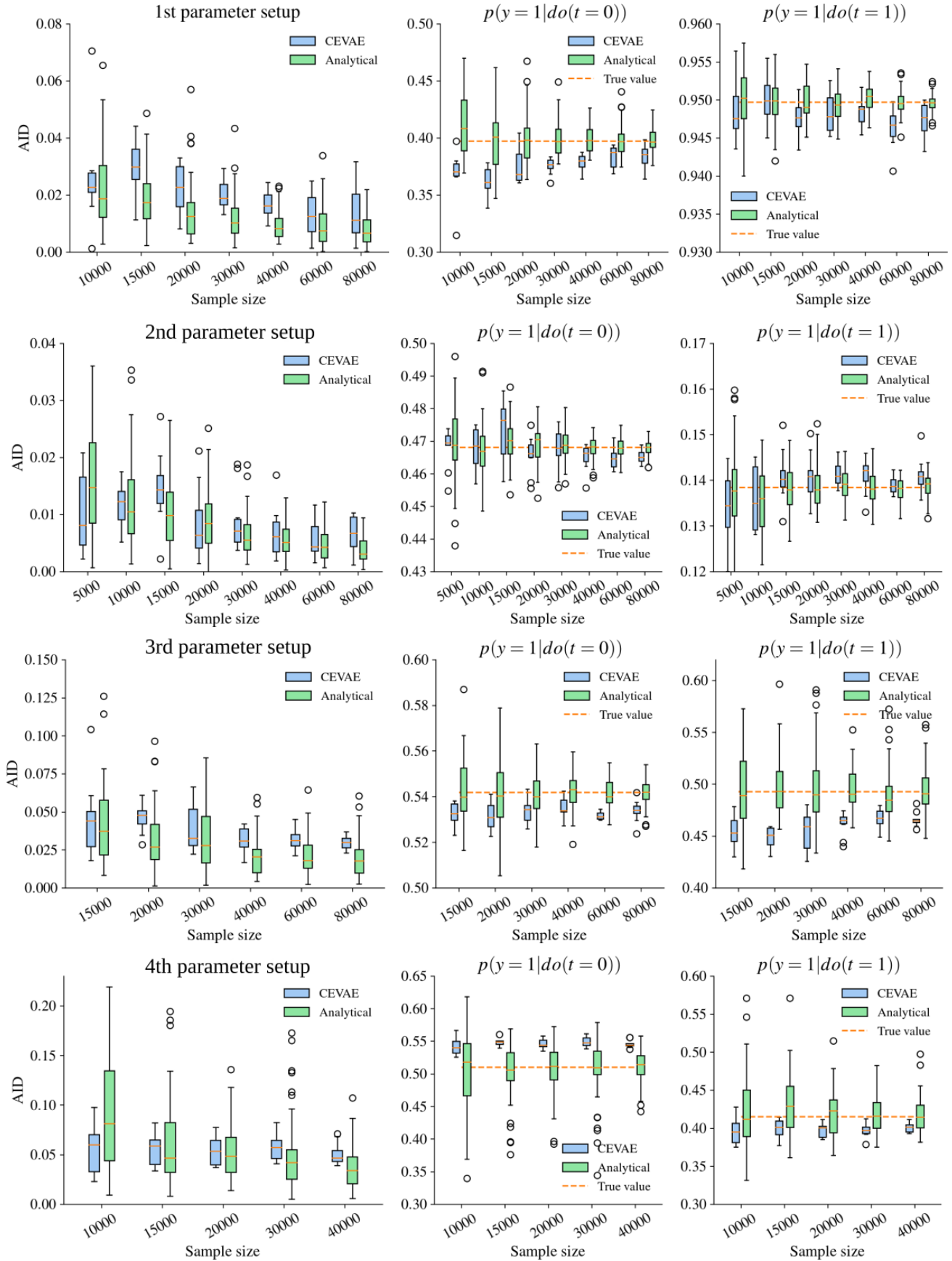


Figure 13. The results from the four additional binary data generating processes. Some outliers are not shown in order to make the plots readable.

Table 2. Data generating parameters for the repeated binary data experiments.

	Process 1	Process 2	Process 3	Process 4
$p(z = 1)$	0.41	0.49	0.42	0.45
$p(x_1 = 1 z = 0)$	0.88	0.24	0.63	0.30
$p(x_1 = 1 z = 1)$	0.66	0.73	0.44	0.44
$p(x_2 = 1 z = 0)$	0.63	0.53	0.81	0.33
$p(x_2 = 1 z = 1)$	0.86	0.63	0.47	0.65
$p(t = 1 z = 0)$	0.51	0.44	0.19	0.25
$p(t = 1 z = 1)$	0.78	0.29	0.64	0.78
$p(y = 1 z = 0, t = 0)$	0.21	0.42	0.49	0.67
$p(y = 1 z = 0, t = 1)$	0.93	0.12	0.72	0.54
$p(y = 1 z = 1, t = 0)$	0.66	0.52	0.61	0.31
$p(y = 1 z = 1, t = 1)$	0.97	0.15	0.18	0.26